ANALYSIS AND SIMULATION OF FAR-FIELD SEISMIC DATA FROM THE SOURCE PHYSICS EXPERIMENT EXPLOSIONS

Robert J. Mellors, Arthur J. Rodgers, Phillip E. Harben, William R. Walter, Sean Ford, Jeffery L. Wagoner, N. Anders Petersson, Bjorn A. Sjogreen, Teresa F. Hauk, Stan D. Ruppert, Stephen C. Myers, Eric M. Matzel, Douglas A. Dodge, Michael E. Pasyanos, and Jon P. Lewis

Lawrence Livermore National Laboratory

Sponsored by the National Nuclear Security Administration

Award No. DE-AC52-06NA25946/NST11-NCNS-TM-EXP-PD15

ABSTRACT

The Source Physics Experiment (SPE-N) at the Nevada National Security Site (NNSS) is planned as a series of chemical explosions under a variety of emplacement conditions. The SPE-N goal is to improve our physical understanding and ability to model how explosion generate seismic waves, particularly S-waves. The first SPE-N explosion (SPE1) occurred in May 2011 and consisted of a 220 lb (100 kg) chemical explosion at a depth of 180 ft (55 m) in granite (Climax Stock). This paper examines the far-field seismic observations and a complementary paper addresses the near-field wavemotion (Antoun et al. [these Proceedings]). The shot was well-recorded by a assortment of over 150 instruments. The greatest density of instruments were located within 5 km of the source but some extended as far out as 20 km, and there are additional local and regional stations that are part of permanent networks. The majority of the SPE-N specific stations were installed as part of 5 radially oriented lines that emanate from the shot location. A variety of instruments were deployed, including high-frequency geophones, accelerometers, broadband seismometers, and rotational sensors. Data recovery from the first shot was over 95%. A review of the SPE1 waveforms shows variations with azimuth in both frequency content and amplitudes. Some of the variations correlated closely with known lateral changes in geology but the nearest stations, all of which were located on granite, also showed significant variations. Preliminary modeling of the SPE1 data using a 3D finite-difference code and a 3D velocity model showed similarities in both arrival times and overall features at low frequencies. Further modeling will be conducted with emphasis on understanding the generation of shear waves and comparison of data with the synthetics. The analysis will also include examination of data from the rotational sensors to characterize the wavefield, P, S, and surface wave amplitudes and amplitude ratios, and comparison to historical data from sources in similar settings.

Note: The Source Physics Experiments at the Nevada Nuclear Security Site (SPE-N) in 2011 should not be confused with the 2003 Source Phenomenology Experiments conducted in Arizona (SPE-A) (Yang and Bonner, 2009).

OBJECTIVES

The SPE-N at the NNSS is a series of chemical explosions intended to enhance our physical understanding and ability to quantitatively model seismic signals from explosions with the goal of improving our nuclear test monitoring capabilities (Brunish et al., 2010). The SPE-N offers a chance to examine broadband explosion seismic signals generated at a wider variety of depths and geologies than exist for local and regional distance nuclear test data.

A particular focus is to use the simulations as a predictive tool in advance of each shot and then to validate the numerical simulations with recorded SPE-N shot data. After each experiment, the codes and models will be refined. The successive iterations will be run in a variety of geological settings and emplacement conditions, with emphasis on understanding the contribution from source and path for each setting and the effect on the observed waveforms. Ultimately, both near-field and far-field simulations will be combined into one comprehensive modeling capability.

The ultimate goal is to be able to model and predict waveform characteristics such as body and surface wave arrival times and amplitudes, P/S ratio, and other aspects of the far-field wavefield. We also hope to address more fundamental questions such as understanding the generation of shear waves and the origin of reversed-polarity Rayleigh waves (Brune and Pomeroy, 1963), which have been previously observed at some hard-rock sites including the nearby HARDHAT and PILEDRIVER shots at NNSS. The SPE-N experiments also serve as a testbed for innovative approaches, such as the use of rotational sensors in resolving and distinguishing shear waves and novel signal analysis techniques using the ambient noise field.

Here we present an overview of the research performed, which included a pre-shot 3D simulation and preliminary examination of amplitudes, rotational sensor performance, and a comparison between the pre-shot synthetics and the observed waveforms. This is followed by an overview of the planned research.

RESEARCH ACCOMPLISHED

This report will focus on the far-field modeling and observations from the first shot, which was intended as a calibration shot and took place on 5/3/11. The 220 lb (100 kg) (chemical explosion) shot was buried at a depth of 180 ft (55 m) in a borehole into the granite Climax Stock and was recorded by a variety of near-field and far-field instrumentation.

Pre-shot Simulation

Prior to the calibration shot, a series of 3D simulations of the far-field wavefield were performed using the WPP finite difference code (Rodgers et al., 2010a). WPP is a second-order node-centered implementation designed specifically for implementation on highly-parallel machines. It models the full wave equation and is capable of handling 3D variations in the material properties (density, compressional and shear velocities), topographic variations on the free-surface, and attenuation. It includes depth-dependent mesh refinement, a variety of source characterizations, and multiple input and output formats (Nilsson et al., 2007; Appelo and Petersson, 2008; Petersson and Sjogreen, 2009; Petersson and Sjogreen, 2010). WPP has been previously used for a variety of seismic wave simulations including earthquakes (Rodgers et al., 2008) and nuclear tests (Rodgers et al., 2010b).

The simulations were conducted on a computational domain of 8 km by 8 km by 5 km over a range of grid spacings. The lowest shear wave velocity was set at 1000 m/s, which is too high for the area; however, this was chosen to avoid very small grid size and hence large computations for this preliminary set of calculations. The smallest grid spacing (5 m) corresponded to an upper frequency of about 13 Hz. Four simulations were run to investigate the effect of 3D layers and topography with respect to a homogenous half-space. Due to the topography and pronounced lateral variations in seismic wave velocities, the inclusion of 3D layers and topography had a dramatic effect on the synthetic seismograms (Figure 2).

Table 1. Material properties in the SPE1 preliminary model

layer	Density (kg/m^3)	Vp (m/s)	Vs (m/s)
Alluvium	2000	1700	1000
Tertiary	2100	2500	1445
preTertiary	2300	4000	2312
Granite	2600	5500	3179

The 3D model was based on a geologic model developed in with EarthVision, a 3D geologic GIS/visualization program (Figure 1; Table 1). A

set of layers corresponding to the topography, Tertiary, pre-Tertiary, and granite stock were converted into a format suitable for WPP with an initial grid spacing of 50 m (which can be interpolated for a finer grid spacings). In this preliminary model, each layer was assigned a fixed base velocity based on previous studies (e.g. Howard, 1985). Later models will incorporate a more realistic base velocity for the alluvium and depth dependence within layers.

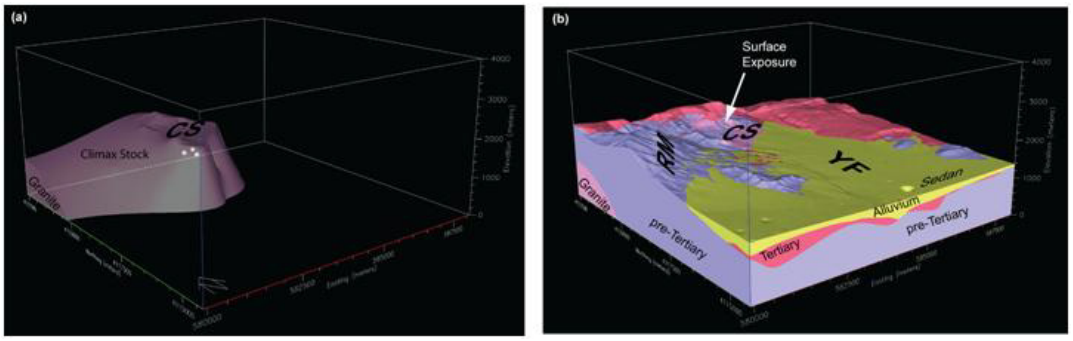

Figure 1. Geologic model used for basis to develop velocity model. A) The 3D representation of the granite Climax Stock, into which the SPE shot was emplaced. The granite is bounded on the south by the low-velocity alluvium underlying Yucca Flat. Most of the remaining area is underlain by Tertiary and preTertiary units.

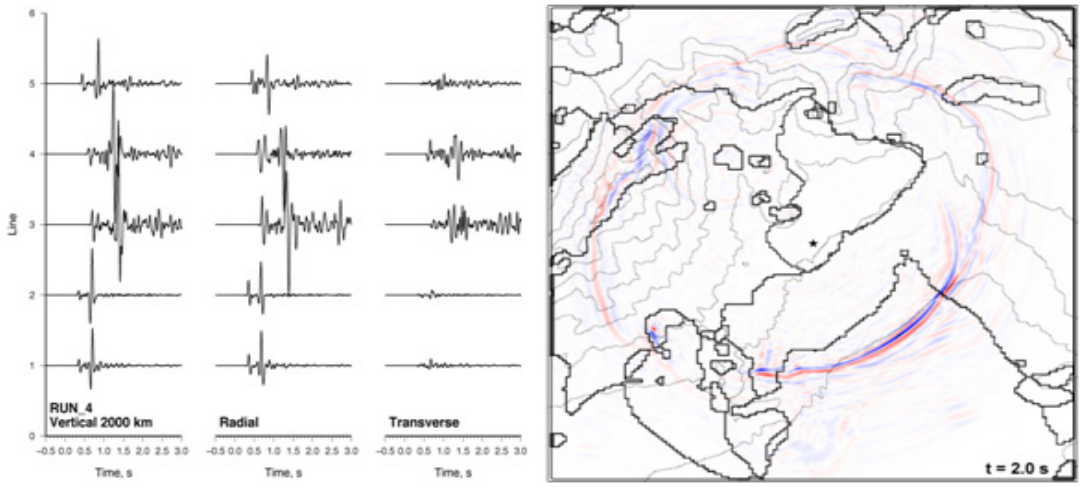

Figure 2. (Left) Synthetic seismograms for each line at the 2 km distance. (Right) Images of the vertical component of ground velocity at 2.0 second after the shot time. The boundary between lithologic units and topographic contour interval (100 m) are indicated by the thick and dotted lines, respectively. See Figure 3 for line positions.

The simulations (see Figure 2) showed that the complex geology and topography of the area is expected to cause strong variations in azimuth in both travel-time and waveform (both amplitude and frequency). In particular, as the seismic waves move to the south and southeast they encounter the low velocities of the Yucca Flat alluvium and underlying tuff. This delays the wavefront relative to the other directions and increases the amplitudes of the Rayleigh waves (Figure 2). This suggests that the complex path geology for lines that extend off the granite would cause a strong effect on the waveforms and greatly increase the complexity of the waveforms.

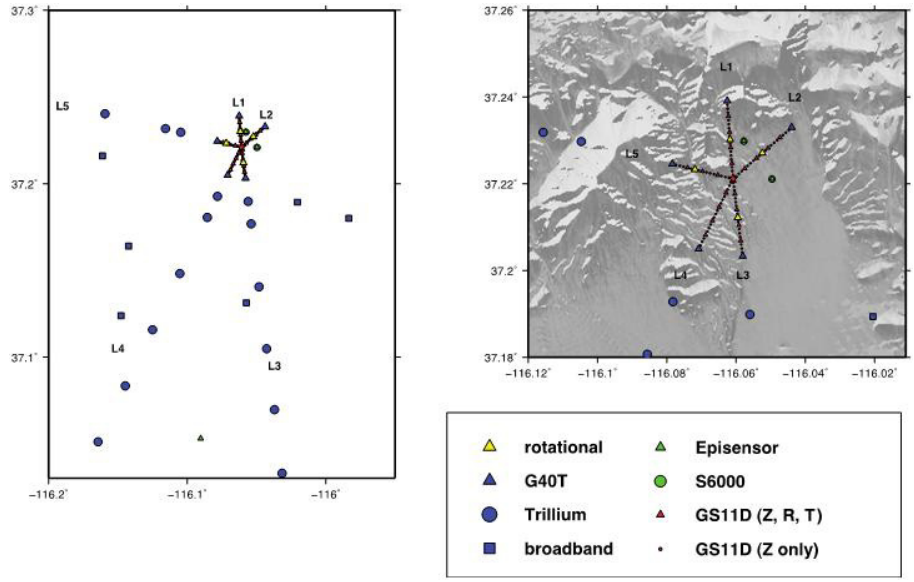

Figure 3. Map of station deployment for the SPE deployment. The map on the left shows the full deployment while the map on the right shows the inner stations and shaded topography.

Data Overview

A variety of instruments were deployed in five lines extending radially away from the shot point. (Figure 3). Nearest the shot point, short-period geophones (GS11) were deployed at 100 m intervals. At the 1 km distance, three-component accelerometers (Kinemetrics Episensors), a rotational sensor (eentec R1), and an additional geophone was installed on Lines 1, 2, 3 and 5. The closely-spaced geophone lines extended out another kilometer and additional instruments (Guralp CMG40T and Nanometrics Trilliums) continued the lines to the south and west (Lines 3,4 and 5). In addition, accelerometers and broadband sensors were deployed at nine other sites away from the lines. These instruments were installed on concrete pads set into the surface. The horizontal components of the instruments were oriented radial and transverse to the shot location. Data recovery was excellent, with over 95% of the possible data recovered. Known issues included sensor and cable problems. Some apparent issues with station locations (possibly due to incorrect cable/channel associations) were also noted.

Clear differences along and between lines were observed (Figure 4 and 5). Lines 3 and 4 were delayed relative to the other lines and strong variations in amplitude and waveforms were observed, with pronounced surface waves visible on Lines 3 and 4, as predicted. Figure 5 shows a selection of seismograms recorded at equal distances for each line and demonstrates the variation in traveltimes between the different lines.

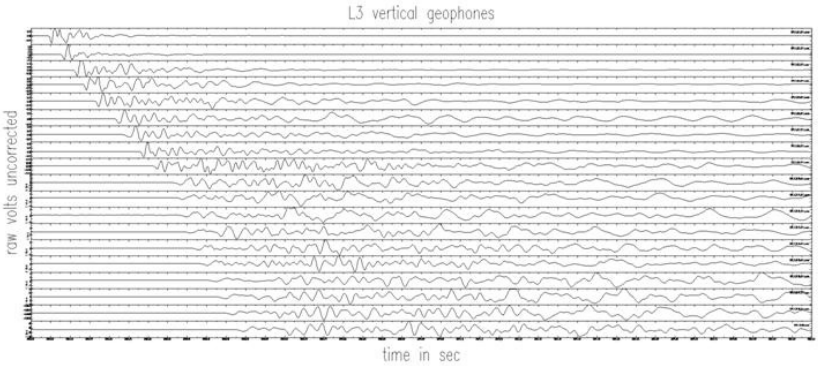

Figure 4. Example of seismograms (vertical component) recorded along Line 3.

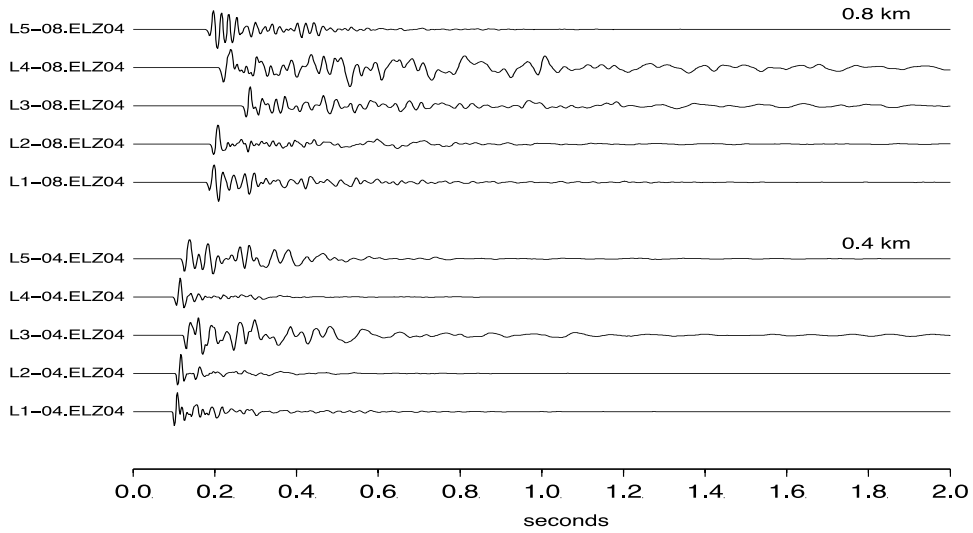

Figure 5. Seismograms recorded at equal distance from the shot location but at different azimuths. Pronounced differences are observed even at these ranges.

Amplitudes

As a quick initial test of the recovery of true ground displacement from the sensors, we measured and compared the first peak-to-peak amplitude of the onset P-waves to amplitudes expected based on refraction shots and given by Kohler and Fuis (1992) as a function of distance (Figure 6). The amplitudes for the SPE1 shot (~100 kg; 220 lbs) roughly corresponded to the expected amplitudes for a shot of that size although considerable scatter is present. Extreme outliers were due to sensors that did not operate correctly. At distances greater than 1 km, an apparent downward trend was visible and may have to do with structural effects on the propagation.

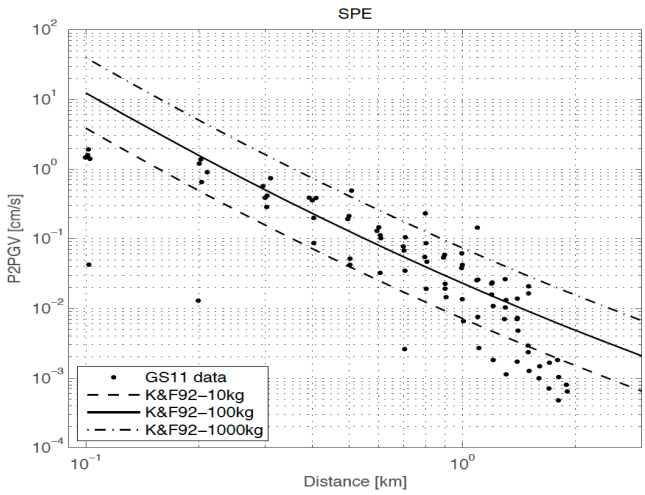

Figure 6. Estimated peak-to-peak amplitudes measured from the first P wave (black dots). Lines indicate values from Kohler and Fuis (1992).

We also looked at the P-wave displacement spectral amplitudes calculated from a very short 0.25 s window starting just before the onset at 5 different azimuthally distributed stations, each 1.5 km from the source (Figure 7). The P-wave spectra show very good signal to noise for this small explosion up to 100-150 Hz depending upon the station. To the extent the source is approximately isotropic there are clear and very strong site effects apparent between stations: amplitude differences of about an order of magnitude between 4 and 20 Hz increasing to nearly two orders of magnitude between 30 and 80 Hz. This is likely a consequence of the shallow sensor deployment and the large variation in the station geology. We plan to analyze ratios between the SPE1 and future explosions in the same borehole so the path and site effects will be in common and cancel out.

In Figure 7 we compare the observations to the Mueller-Murphy (Mueller and Murphy, 1971) predictions for granite using the parameters given by Stevens and Day (1985). The observed ground motions are larger even figuring in an explosive yield twice as large to account for difference between chemical and nuclear explosions observed in the 1993 Non-Proliferation Experiment (NPE). We have included a nominal factor of 5 amplitude increase across all frequencies as a crude site effect and applied a nominal frequency dependent attenuation to the theoretical spectra plotted in Figure 7. The observed spectra span the expected SPE1 corner frequency near 35 Hz. For comparison we also show the Mueller-Murphy theoretical spectra for the next planned shot in the same location (SPE2, approximately 1000 kg). Observed spectra for SPE2 are expected to increase over the observed SPE1 spectra approximately as the ratio of the theoretical models.

P/S Amplitude Ratios as an Earthquake-Explosion Discriminant

The NNSS is located in an active seismic area, which opens the possibility of recording and analyzing earthquakes on the same sensors deployed for the SPE-N shots. So far we have only examined a few days of continuous data and compared them to the seismic catalog compiled by the University of Nevada-Reno Seismological Laboratory. We found one probable magnitude 0.7 earthquake in this catalog located about 8 km north of the SPE1 borehole that has good amplitude signals, similar to the SPE1, recorded on most of the same stations. By comparing the signals at a sensor that is approximately the same epicentral distance of 8-9 km from both events we can perform a local very high frequency earthquake/explosion comparison to look for similarities and differences. Seismograms from both events on a common station geophone are shown in Figure 8 in four different frequency bands. The probable earthquake shows a much clearer S-phase about 2 seconds after the small P arrival in all filter bands, in contrast to the explosion where the S-wave arrival is not very clear. The earthquake also shows larger S-wave amplitudes, giving it a smaller P/S ratio than the explosion at all frequency bands, above and below the explosion corner frequency (expected around 35 Hz). These P/S amplitude ratios have been used to identify explosions and discriminate them from earthquakes, but without a very clear physical understanding of how explosions generate S-waves. This reduces our ability to predict P/S behavior across frequency bands. A better physical understanding leading to predictive modeling capability for explosion P/S ratios is one of the main objectives of the SPE-N project. We expect to examine this and other probable earthquakes on the SPE-N seismic network, allowing us to compare and contrast different source types as part of the project.

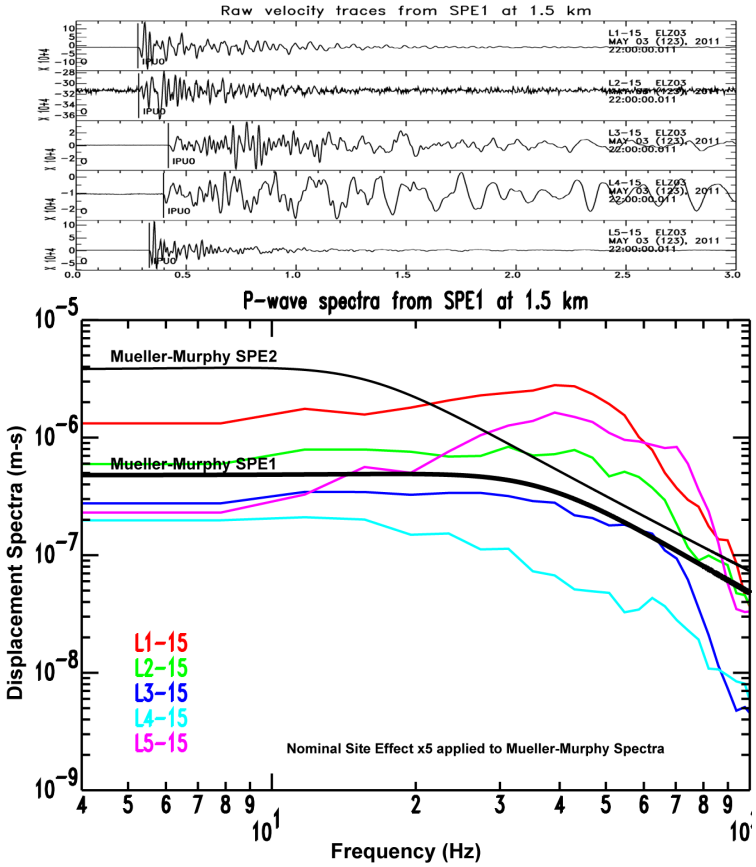

Figure 7. (Top) Seismograms recorded at a distance of 1.5 km. (Bottom) Corresponding P-wave spectra compared with the expected Mueller-Murphy model at a distance of 1.5 km.

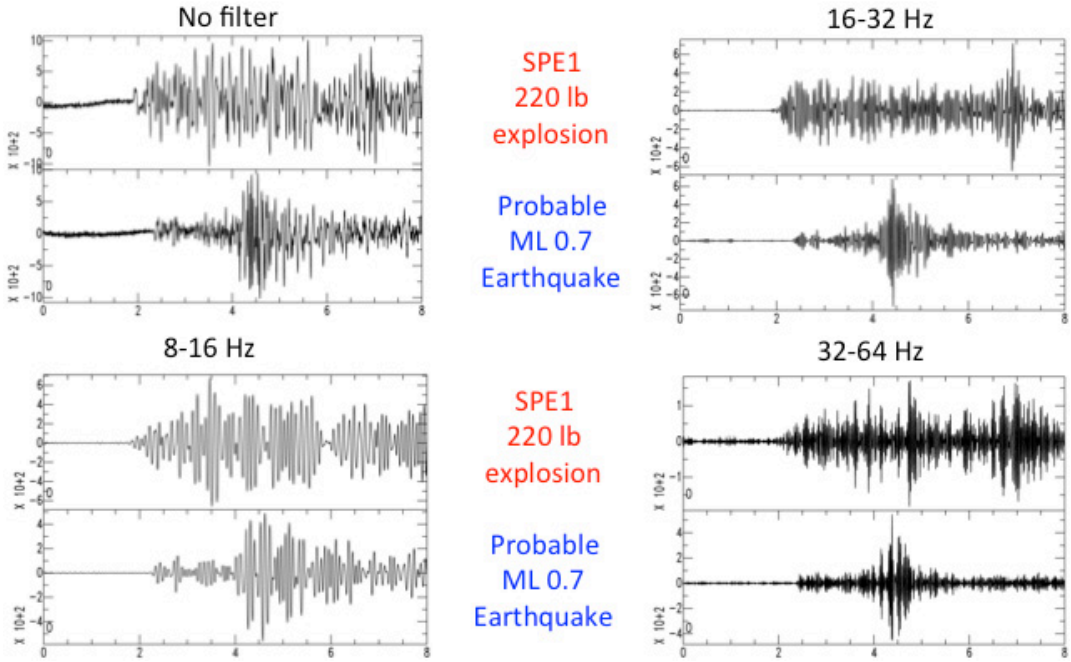

Figure 8. Comparison of SPE1 explosion and small local earthquake at similar distances.

Rotational Sensors

Four rotation sensors were deployed at a distance of 1 km from the shot to investigate their utility in measuring and characterizing shear waves. In theory, rotational sensors should be sensitive only to shear waves and therefore should be useful in distinguishing between P and S wave energy. Standard (orthogonal-component) accelerometers were located at the same sites.

For a plane wave without scattering, the rotation rate about the Z-axis will be in-phase with the transverse acceleration (e.g., Wang et al., 2009; Schreiber et al., 2009). Given the relatively short distance (1 km) from the SPE1 the plane wave assumption is not perfectly satisfied. Instrumentation effects (cross-axis coupling, non-linear response) may also play a role.

The waveform correlation is remarkably good (Figure 9) and interestingly, clear correlation exists at the onset of the signal. Although the range is only 1 km and there is very little time between the P and S arrival times in the record, an uncorrelated signal would be expected between the two sensor components during the P-phase onset because the P should be purely translational and hence invisible to a rotational sensor. Two factors might cause correlation of the sensor components to be correlated during the P-phase: rotational sensor sensitivity to translational motion and P-to-S scattering along the path allowing S-wave energy to arrive at the station during the P-wave coda. Previous tests of the R1 sensors to linear cross-axis sensitivity (Nigbor et al., 2009) suggested values of about 0.5 milliradian/sec/(m/sec/sec), which, when corrected for the ground motion observed during the SPE1, would indicate less than 2% cross-axis coupling which is insufficient to explain the apparent P wave correlation.

To test the possibility of S-wave energy arriving in the P-wave coda due to along-path scattering, possibly at the granite/alluvium interface, the vertical and horizontal channels of the accelerometer are examined. On the L2 line, the vertical component shows a signal arriving approximately 4 msec before the horizontal component. This tends to support the idea of P-to-S conversion near the station. On the L5 line a lag between the horizontal and vertical components is not as clear.

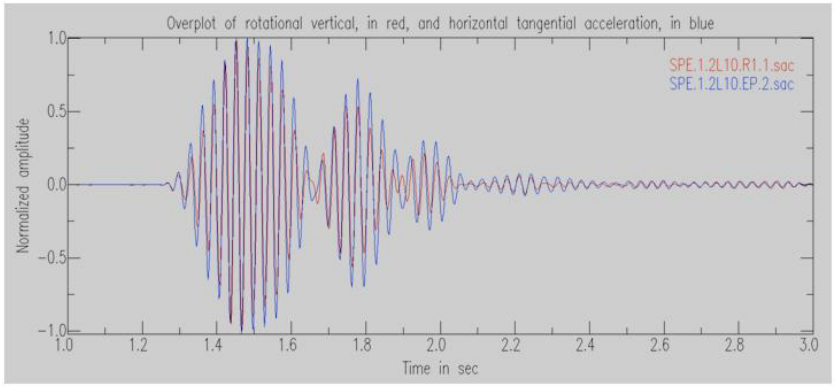

Figure 9. Rotational sensors (red) from Line 2. The blue line shows the transverse component of the accelerometer (Episensor) at the same site. Data have been bandpassed filtered (25 to 35 Hz) and amplitudes have been normalized.

Comparison with synthetics.

A comparison of the synthetics generated by the pre-shot modeling with the observed data (Figure 10) yields interesting similarities and differences. For example, the modeled synthetics (Figure 2) predicted traveltime delays for Lines 3 and 4 together with increased complexity and higher amplitude surface waves. These features are present in the data. Figures 5 and 7, which show seismograms recorded at distances out to 1.5 km, show approximately the same characteristics as the synthetics. Lines 3 and 4 are delayed while Lines 1, 2, and 5 possess similar travel times and generally simpler waveforms. However, the predicted traveltimes, while relatively similar, do not match the observed traveltimes exactly. This is presumably due to systematic bias in the model. Nor do the synthetics capture the full complexity of the data. In particular, they fail to reproduce the longer period surface waves that are clearly evident on Lines 3 and 4. As noted above, these synthetics used an arbitrary lower cutoff of 1000 m/s for the shear wave speed to reduce computational time in the preliminary tests. This likely resulted in the poor match of the surface wave at longer distances. This is more obvious for lines 3 and 4, which cross the alluvium (underlain by tuff) of Yucca Flat. Improving the model to remove bias and better match the data is one of our first tasks.

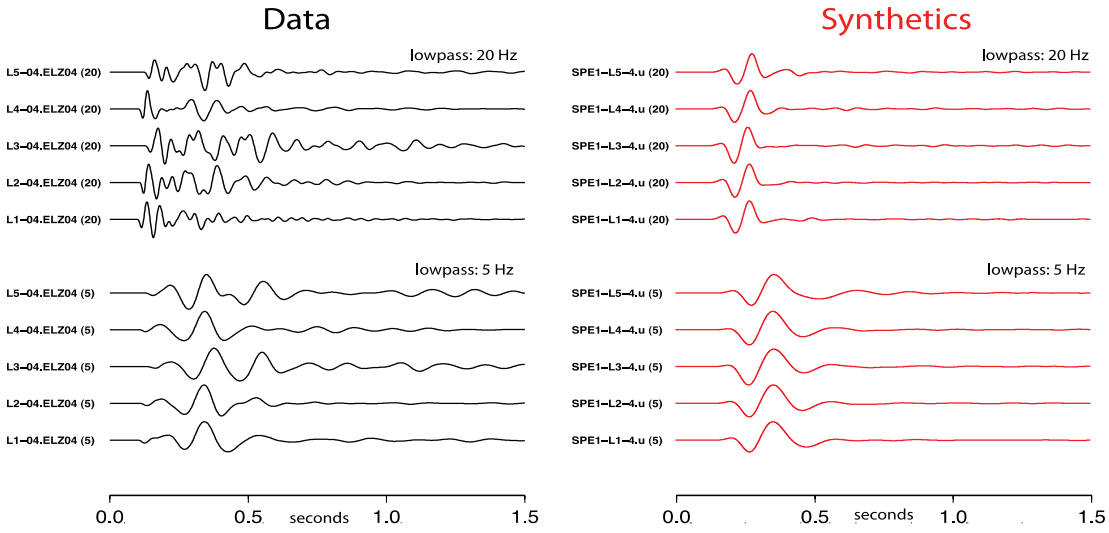

Figure 10. Lowpass-filtered data (left) with synthetics (right) for stations at 0.4 km.

It is useful to filter the data to gain a better idea of the differences. We note at this point that the data have not been corrected for instrument response. In general, the fit is better at lower frequencies. Figure 10 shows both the data and the synthetics low-passed filtered at 5 and 20 Hz. At 5 Hz, which is well within the expected frequency range of the synthetics (up to 13 Hz), lines 1, 2, and 4 roughly resemble the synthetics. We suspect that this is likely due to path differences as, at this distance (400 m), these are the stations that are still on the same granite stock as the shot. Line 3 reaches the southern edge of the granite quickly. As the Climax Stock is bounded by the Yucca Fault on this side, the boundary between granite and alluvium is abrupt.

Ambient Noise Cross-correlation

Ambient noise cross-correlation was tested using various combinations of instruments, both geophones and broadband instruments. Figure 11 shows an example based on data recorded by the L3 line over a period of 8 days. It was filtered between 2 and 8 Hz before correlation. At short distances (less than 300 m) the noise is highly correlated at these frequencies. At longer distances the high frequency signal is just beginning to emerge from the noise and should be well defined once more data are included in the correlation stacks. Lower frequencies are possible using the broadband data.

With additional continuous data, we anticipate that this procedure will yield dispersion curves, which can be used to constrain the shallow velocity model and therefore will be useful in improving the 3D seismic model used in the finite difference modeling.

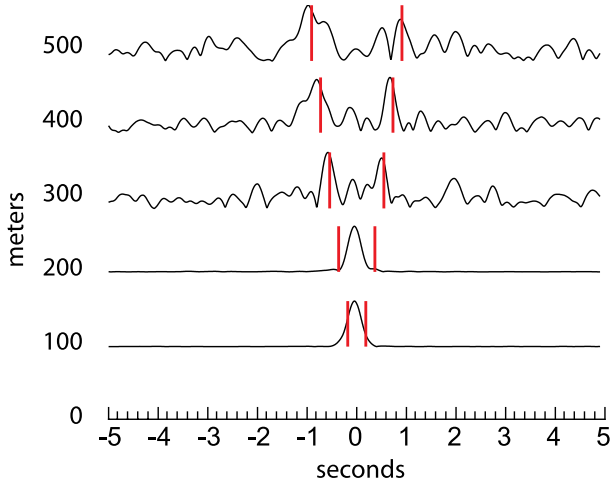

Figure 11. Envelopes of the estimated Greens functions (EGF) calculated using the ambient noise cross correlation technique on geophone (GS11) data. The red lines mark group velocities of +-0.55 km/s to emphasize peaks.

CONCLUSIONS AND RECOMMENDATIONS

Initial analysis is proceeding and the abundant data return ensures that more analysis will be forthcoming. The next steps will include a revision of the model to allow for more realistic velocity structure. We will also use results from the near-field models to improve the source time functions and amplitudes. Initial results from the near-source models and data suggest that considerable variability with azimuth occurs near the source and this might translate to variations in the far-field. We intend to couple the near-field and far-field modeling to help resolve this question and to distinguish between source and path effects.

A full suite of other analysis will be conducted. This will include further study of the rotational data and modeling, as well as examination of the P, S wave spectra and ratios, body and surface wave amplitudes, cross-correlation and location analysis, and comparison with historical data. The ultimate goal is to be able to predict signals and monitoring algorithms derived from them using the physics-based coupled modeling codes. The SPE-N data serve as critical development and validation data for this purpose. This new capability will lead to improved algorithms and better monitoring capabilities, particularly for regions lacking empirical explosion data.

ACKNOWLEDGEMENTS

We thank NA-22 and all the SPE-N participants for all their efforts in planning and carrying out SPE1. We thank the group at NSTec and in particular Bob White and Catherine Snelson-Gerlicher for their efforts in organizing and collecting the data. Rob Abbott was also very helpful. Ken Smith assisted with data organization. Numerical simulations were performed on the SIERRA Linux cluster operated by Livermore Computing using a Computing Grand Challenge Allocation.

REFERENCES

Antoun, A., X. Heming, O. Y. Vorobiev, E. B. Herbold, L. Glenn, and I. Lomov (2011). Analysis and simulation of near-field wave motion data from the source physics explosions, these Proceedings.

Appelo, D. and N.A. Petersson (2008). A stable finite difference method for the elastic wave equation on complex geometries with free surfaces, *Comm. Comput. Phys*., 5: 84–107.

Brune, J. and P. W. Pomeroy, (1963). Surface wave radiation patterns for underground nuclear explosions and small magnitude earthquakes, *J. Geophys. Res*. 68: 5005–5028.

Brunish, W. N., W. L. Hawkins, D. Coblentz, H. J. Patton, J. J. Zucca, J. J. Sweeney, C. R. Carrigan, T. H. Antoun, C. E. Seifert, K. H. Wohletz, C. R. Bradley, A. J. Sussman, T. W. Bowyer, R. Cirbell, C. M. Snelson, and P. Lee, (2011), Source Physics Experiments at the Nevada Test Site, *Proceedings of the 2010 Monitoring Research Review: Ground-Based Nuclear Explosion Monitoring Technologies*, Vol. 1, LA-UR-10-05578, pp. 370–390.

Howard, N. (1985). Variation of properties of nuclear test areas and media at the Nevada Test Site, LLNL Technical Report, UCRL-53721.

Kohler, W. M., and G. S. Fuis (1992). Empirical dependence of seismic ground velocity on the weight of explosives, shotpoint site condition, and recording distance for seismic-refraction data, *Bull. Seismol. Soc. Am*. 82: 2032–2044.

Nigbor, R.L., J.R. Evans, C.R. Hutt, (2009). Laboratory and field testing of commercial rotational seismometers, *Bull. Seismol. Soc. Am.* 99: 1215–1227.

Mueller, R. A. and J. R. Murphy (1971). Seismic characteristics of underground nuclear detonations. Part I. Seismic spectral scaling, *Bull. Seismol. Soc. Am*. 61: 1975.

Nilsson, S., N.A. Petersson, B. Sjogreen, H.-O. Kreiss (2007). Stable difference approximations for the elastic wave equation in second order formulation, SIAM *J. Numer. Anal*. 45: 1902–1936.

Petersson, N. A., and B. Sjogreen (2009). An EnergyAbsorbing Far-Field Boundary Condition for the Elastic Wave Equation, LLNL-JRNL-405423, *Comm. Comput. Phys*. 6, 3: 483–508.

Petersson, N. A., and B. Sjögreen (2010). Reference guide to WPP version 2.0, Lawrence Livermore National Laboratory technical report, LLNL-TR-422928.

Rodgers, A., A. Petersson, S. Nilsson, B. Sjogreen and K. McCandless (2008). Broadband Waveform Modeling of Moderate Earthquakes in the San Francisco Bay Area to Evaluate the USGS 3D Seismic Velocity Model, *Bull. Seismol. Soc. Am*. 98: 969–988.

Rodgers, A. J., J. Wagoner, N. A. Petersson and B. Sjogreen (2010a). Pre-shot simulations of far-field ground motions for the source physics experiment (SPE) explosions at the Climax Stock, Nevada National Security Site, technical report, Lawrence Livermore National Laboratory, LLNL-TR-461990

Rodgers, A., N. A. Petersson, B. Sjogreen (2010b). Simulation of topographic effects on seismic waves from shallow explosions near the North Korean Nuclear Test Site with emphasis on shear wave generation, in press *J. Geophys. Res.-B Solid Earth Planets*, doi:10.1029/2010JB007707, LLNL-JRNL-433892.

Schreiber, K.U., J.N. Hautmann, A. Velikoseltsev, J. Wassermann, H. Igel, J. Otero, F. Vernon, and J.R. Wells (2009). Ring laser measurements of ground rotations for seismology, *Bull. Seismol. Soc. Am*. 99: 1190–1198.

Stevens, J. L. and S. M. Day (1985). The physical basis of mb:Ms and variable frequency magnitude methods for earthquake/explosion discrimination, *J. Geophys. Res*. 90: 3009–3020.

Tarabay, A., X. Heming, O. Y. Vorobiev, E. B. Herbold, L. Glenn, and I. Lomov (2011). Analysis and simulation of near-field wave motion data from the source physics explosions, these Proceedings.

Wang, H., H.Igel, F. Gallovie, A. Cochard, (2009), Source and Basin Effects on Rotational Ground Motions: Comparison with Translations, *Bull. Seismol. Soc. Am*. 99, No. 2B: 1162–1173.

Yang, X. and J. L. Bonner (2009). Characteristics of chemical explosive sources from time-dependent moment tensors, *Bull. Seismol. Soc. Am*. 99: 1, 36–51.